Journal of Structural Geology 43 (2012) 63–72

Contents lists available at SciVerse ScienceDirect

Journal of Structural Geology

journal homepage: www.elsevier.com/locate/jsg

Preferential cataclastic grain size reduction of feldspar in deformation bands in poorly consolidated arkosic sands

Ulrike Exner [a,b,*], Cornelius Tschegg [c]

[a] Natural History Museum Vienna, Burgring 7, 1010 Vienna, Austria
[b] Department of Geodynamics and Sedimentology, University of Vienna, Althanstrasse 14, 1090 Vienna, Austria
[c] Department of Lithospheric Research, University of Vienna, Althanstrasse 14, 1090 Vienna, Austria

ARTICLE INFO

Article history:
Received 9 January 2012
Received in revised form
1 August 2012
Accepted 3 August 2012
Available online 10 August 2012

Keywords:
Cataclasis
Porosity
Microstructure
Fault sealing

ABSTRACT

This study presents microstructural as well as bulk and mineral chemical investigations of deformation bands in uncemented, friable arkosic sands of Miocene age (Vienna Basin, Austria). Our microstructural study indicates grain size reduction by grain flaking in deformation bands with small offsets (0.5–8 cm), and dominant intragranular fracturing and cataclasis of altered feldspar grains at larger displacements (up to 60 cm). Relative to quartz, the sericitized feldspar grains are preferably fractured and abraded, which additionally leads to an enrichment of mainly phyllosilicates by mechanical expulsion from feldspar. Both cataclasis of quartz and feldspar grains and enrichment of phyllosilicates result in grain size reduction within the deformation bands. The measured reduction in porosity of up to 20% is in some cases associated with a permeability reduction, reflected in the retention of iron-oxide rich fluids along deformation bands. These deformation bands formed at very shallow burial depths in unconsolidated sediments indicate that fault sealing may occur in the absence of chemical alteration of the deformation bands and lead to a compartmentalization of a groundwater or hydrocarbon reservoir.

1. Introduction

Many hydrocarbon reservoirs are located in high-porosity, terrigeneous sediments, sealed by either stratigraphic or tectonic zones of low porosity (Allen and Allen, 2005). It has been recognized that in unconsolidated sediments deformed at shallow burial depth (ca. <1 km) zones of localized deformation do not develop as macroscopically detectable fractures along which cohesion is lost, but rather as tabular zones of reorganized or crushed grains, commonly described as deformation bands (e.g. Aydin, 1978; Fossen et al., 2007). In many cases, these fault rocks do not serve as fluid pathways, but rather inhibit the flow of fluids (Sigda et al., 1999; Eichhubl et al., 2004; Sternlof et al., 2006). The processes of porosity reduction in near-surface fault zones comprise compaction by grain rotation and reorganization, preferential cementation, clay smearing, and cataclastic grain size reduction (Fisher and Knipe, 1998). Phyllosilicate grains with high aspect ratios are usually aligned parallel to the shear vector in a fault zone. Furthermore, clay minerals may preferentially be generated or precipitated in deformation bands and fault zones in granular sediments, due to the migration of fluids or infiltration of clay sized particles and preferred capturing due to the low porosity and permeability (Aydin et al., 2006).

Only a limited number of studies presented microstructural investigations of porosity-reducing processes in friable sediments (e.g. Cashman and Cashman, 2000; Rawling et al., 2001; Rawling and Goodwin, 2003; Balsamo and Storti, 2010; Tueckmantel et al., 2010). Microstructures were investigated mostly from naturally (e.g. Antonellini et al., 1994; Eichhubl et al., 2004; Sternlof et al., 2005) and experimentally (e.g. Haied and Kondo, 1997; Baud et al., 2000; El Bied et al., 2002; Baud et al., 2004) deformed quartz-dominated or monomineralic quartz sandstones, or from clay mineral rich shales (e.g. Eichhubl et al., 2005), but not from feldspar rich sediments.

Grain size analysis and microstructural studies of faults and deformation bands in seismically active segments of the San Andreas Fault revealed that cataclastic deformation may occur in unconsolidated sediments even at negligible burial depth (Cashman and Cashman, 2000; Cashman et al., 2007). Investigating experimental and natural microstructures, several authors proposed that both increasing normal stress comparable to overburden pressure and shear displacement leads to more intense

* Corresponding author. Natural History Museum Vienna, Burgring 7, 1010 Vienna, Austria. Tel.: +43 1 52177 254; fax: +43 1 52177 459.
E-mail addresses: ulrike.exner@nhm-wien.ac.at, ulrike.exner@univie.ac.at (U. Exner), cornelius.tschegg@univie.ac.at (C. Tschegg).

0191-8141
http://dx.doi.org/10.1016/j.jsg.2012.08.005

grain fracturing and localization of displacement in narrower zones (Rawling and Goodwin, 2003; Torabi et al., 2007). Grain flaking and intragranular fracturing (i.e. fractures cutting across an entire grain) were identified as the main source of grain size reduction and thereby porosity reduction, already in deformation bands and faults with very low shear displacement of a few centimeters (Torabi and Fossen, 2009). It was suggested that weaker feldspar grains and lithic fragments are subjected to grain fracturing at lower confining pressure (<20–30 MPa or less than 1 km of overburden) than quartz grains (Sigda et al., 1999; Rawling and Goodwin, 2003), and thus lead a selective grain size reduction of these weak grains by chipping and cataclasis already at low burial depth.

Commonly it is assumed that porosity and permeability reduction in unconsolidated sands containing lithic fragments is achieved by flaking of strong grains or intragranular fracturing of weaker particles, sometimes associated with the infiltration or growth of clay minerals (e.g. Balsamo and Storti, 2011). Several studies propose that the degree of transgranular fracturing can be related to the normal stress during deformation, as well as to increasing shear strain (e.g. Marone and Scholz, 1989; Torabi et al., 2007).

In the present study we show an example of deformation bands in shallowly buried arkosic sands, where grain size- and permeability reduction is evident in the field. By microstructural, bulk and mineral chemical analyses, we demonstrate that with increasing shear strain preferential cataclasis of sericitized feldspar leads not only to a general grain size reduction, but also to preferential enrichment of phyllosilicates in the matrix, which could have consequences for fault sealing and compartmentalization of hydrological or hydrocarbon reservoirs.

2. Geological setting and outcrop description

The sampling site is located at the northern margin of the Eisenstadt-Sopron Basin (Fig. 1), a satellite basin of the Vienna Basin, Austria (Royden, 1985), where deformation bands are abundant along the basin margin in various lithologies (Exner and Grasemann, 2010; Rath et al., 2011). At the studied outcrop in a sand pit near Eisenstadt (Fig. 1) numerous conjugate deformation bands document an extensional deformation related to the nearby Eisenstadt Fault, where some 80 m of dip slip displacement down to the southeast are recorded (Fodor, 1995). The Miocene sediments comprise coarse, friable sands, which can be easily removed by

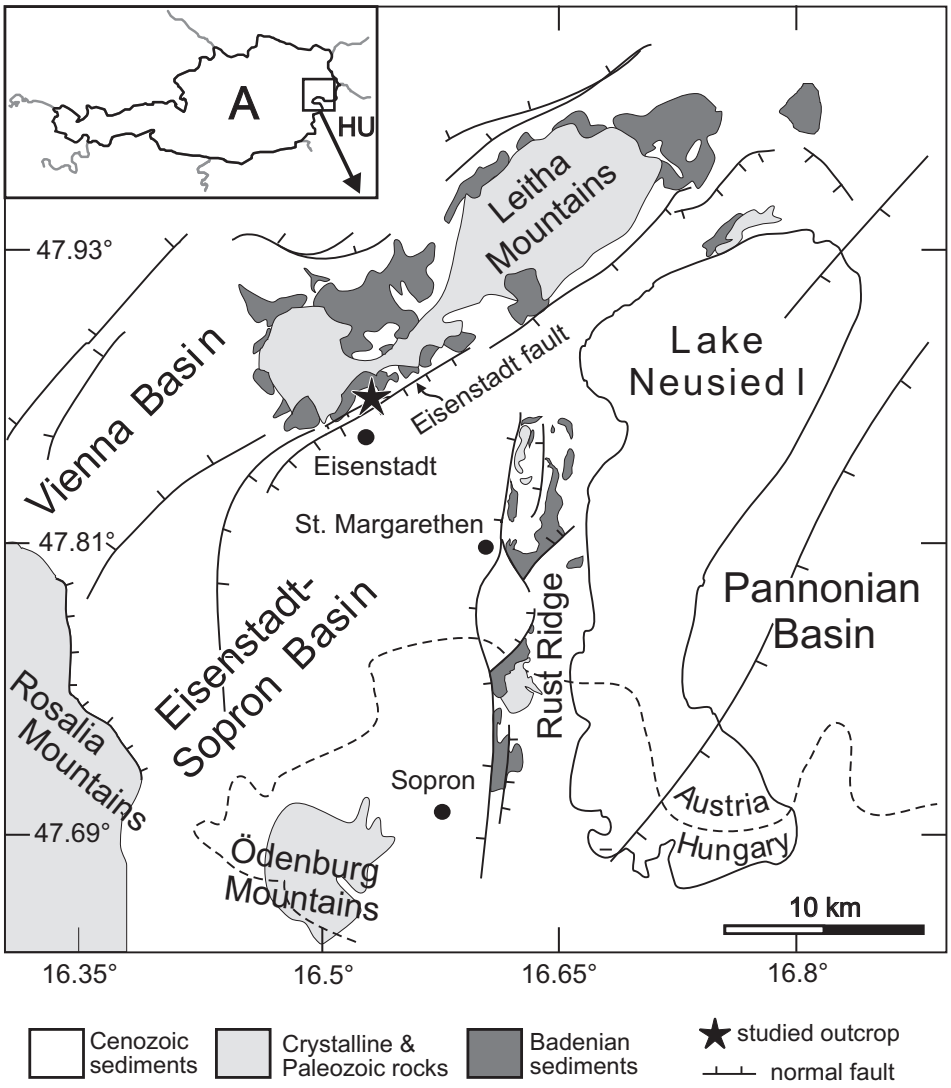

Fig. 1. Location of the studied outcrop at the northern margin of the Eisenstadt-Sopron basin, in the footwall of the Eisenstadt Fault (modified after Schmid et al., 2001).

hand, with intercalated layers and channels of gravels, and are interpreted as fluvial deposits reworked in a shallow marine environment (Sauer et al., 1992). The components are derived from greenschist to amphibolite facies lithologies, eroded from the nearby located metamorphic basement rocks, i.e. predominately orthogneisses, biotite-schists, amphibolites and quartzites (Brix and Pascher, 1994).

Deformation bands occur as conjugate, NNE–SSW trending planar zones protruding from the surrounding undisturbed sediment (Fig. 2). The amount of displacement accumulated along the bands as well as the degree of localization is highly variable within the outcrop. Deformation bands with displacements of some few cm (0–8 cm) are developed as 1–3 cm thick, tabular zones of distributed deformation. Larger displacement is accumulated along subparallel or anastomosing strands of deformation bands, forming up to approximately 1 m broad zones with up to 1.5 m of normal offset (Fig. 2). Alternatively, some narrow zones of maximum 2–5 cm thickness also record larger displacements (~10–60 cm) and show macroscopic evidence of grain size reduction, since they contain much finer grained material than the surrounding sediment. Only one mature fault zone with a well-developed fault core, striated slip surfaces and a displacement larger than 60 cm was identified in the southern part of the exposure (Sauer et al., 1992), which is however not in the scope of this paper.

For this study we selected deformation bands with a displacement of 2–8 cm (STG06 in Fig. 3a), bands with a displacement of ca. 60 cm (STG07 in Fig. 3a), as well as the respective undeformed host sediment. Although the original definition of deformation bands is restricted to features with some few mm of displacement (Aydin, 1978), we use the term deformation bands also for the structures with large displacement, as they neither show slickenside lineations nor open fractures or joints but a gradual transition to the undeformed host sediment. However, we avoid the term clusters of deformation bands, since the samples chosen in this study are characterized as narrow features, instead of being a zone of several discernible and anastomosing bands (e.g. described by Fossen et al., 2007). The samples are taken from areas with macroscopically discernible sedimentary bedding defined by variations in grain size from fine to coarse sand, or alignments of larger pebbles (Fig. 3a). Silt or clay layers are absent along the sampled deformation bands, and no cementation can be recognized macroscopically. In many places the original light-gray color of the shallow marine sands is stained by brownish iron hydroxides occurring in patches parallel or oblique to the sedimentary layering. The staining clearly postdates the deposition of the sequence and even the activity of the deformation bands, as it is not offset by the bands but remains within one level irrespective of composition or displacement (Fig. 3a). Some of the conjugate deformation bands form barriers for the iron hydroxide rich fluids, which is documented by the absence of staining in the footwall of the bands (Fig. 3b).

3. Methods

During suitable weather conditions well below freezing temperature of water (ca. −10 °C), we sampled the coarse, friable sands by carefully sprinkling water onto the area of interest. After some few minutes, the uppermost 2–4 cm of the sample were fixated by the water now crystallized to ice, and could be removed from their position without internal destruction. In order to protect the samples from disaggregation during transport to the lab, they were embedded in a plaster bandage, with the top left uncovered to permit later dehydration. After drying, the samples were saturated with resin in order to maintain their original texture and to enable further thin section preparation. The observed microstructures, revealing significant differences in grain size and fracture types between the host sediment and the deformation bands, indicate that the applied sampling technique perfectly preserves the sedimentary and deformation related fabrics.

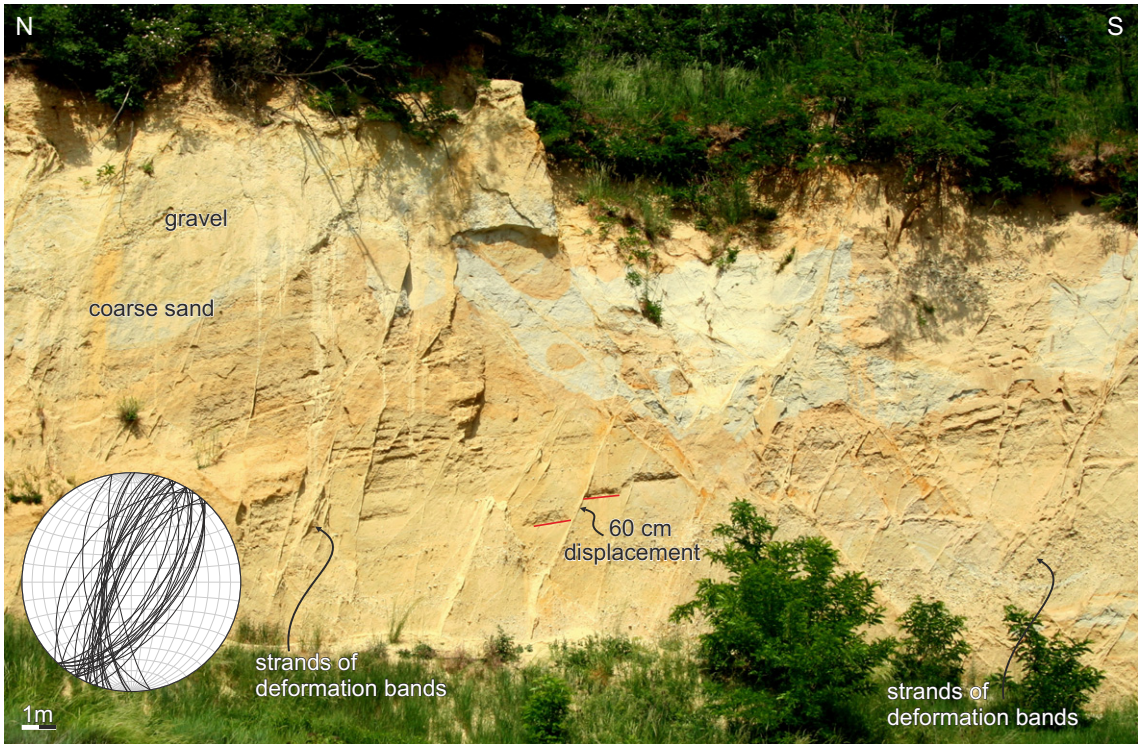

Fig. 2. Overview of the studied outcrop, displaying closely spaced sets of conjugate NNE–SSW trending deformation bands with normal offset. Inset showing orientation of deformation bands (equal area projection, lower hemisphere).

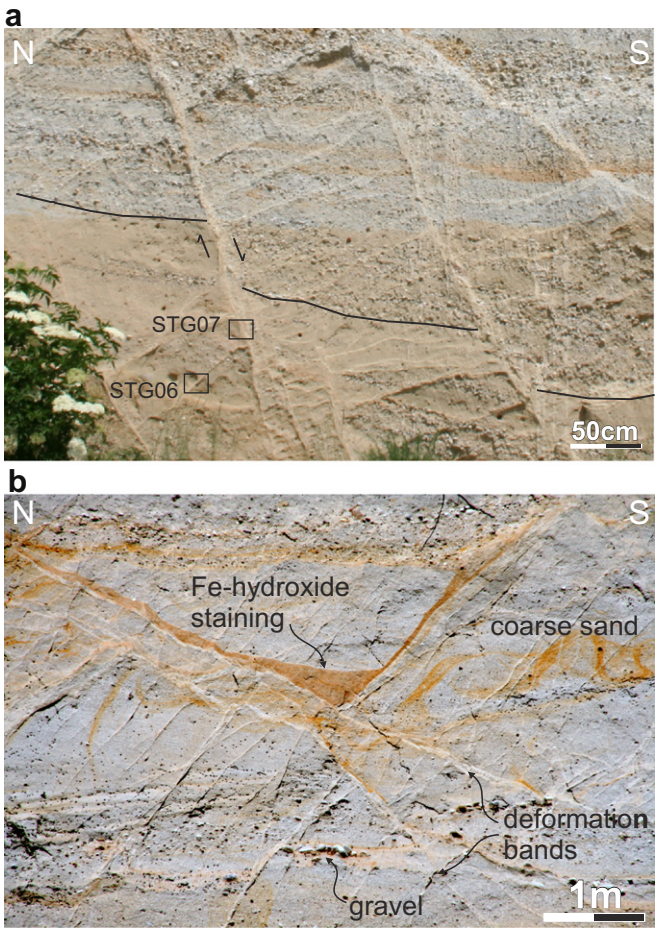

Fig. 3. a) Two of the sampled deformation bands with 2 cm (STG06) and 60 cm (STG07) offset. Displaced gravel bed is indicated. Note the Fe-hydroxide staining in the lower part of the section, with a horizontal border toward the original gray coloring, not being displaced by the deformation band. b) Iron-rich fluids trapped between a set of conjugate deformation bands, evident from Fe-hydroxide staining in the hanging wall.

Polished thin sections were carbon-coated and analyzed with a Cameca SX100 electron microprobe (EPMA) equipped with four wavelength dispersive and one energy dispersive spectrometers (Department of Lithospheric Research, University of Vienna). To gain high resolution back-scattered electron (BSE) images in an appropriate size (up to 5 mm wide), numerous pictures were acquired and stitched together automatically, using an instrumental integrated method. Working conditions for mineral analyses were set to 15 kV acceleration voltage and 20 nA beam current; qualitative analyses were made against natural standards. Porosity and bulk grain size distributions were measured on binary images obtained from BSE images using the software ImageJ. Grain size distributions are plotted following the procedure of e.g. Torabi et al. (2007), as log exceedence frequency versus particle size area. Best fits for the power law distributions are described by the exponent *D*, which is given as two-dimensional (since extracted from 2D cross sections of the 3D grains), but could simply converted to three dimensions by adding 1 (e.g. Blenkinsop, 1991). We use the two-dimensional exponent throughout this study, also when comparing our values with data from the literature.

For the separate grain size analysis of quartz and feldspar, element maps (Si, Al, K, Na, Ca, Mg and Fe) were acquired on an FEI QuantaTM 3D FEG (Department of Lithospheric Research, University of Vienna). The EDAX Genesis phase cluster analysis tool combines BSE images, element maps and spectral information for each pixel to create a phase map instead of separate element maps, which allows for an extraction of individual phases from the images to calculate grain size distributions for the two minerals of interest separately.

In order to gain bulk major and trace element compositions of deformation bands and adjacent host rocks, a representative amount (>200 g) of sediments was probed and analyzed with a Phillips PW2400 X-ray fluorescence spectrometer (Department of Lithospheric Research, University of Vienna). For major elemental composition, fused beads (1× sample:5× flux) and for trace element analysis pressed powder pills were prepared.

4. Results

4.1. Microstructures and mineral composition of the host sediment

The host sediment consists mainly of 20–2000 μm (but in gravel beds up to 5 cm) sized rock fragments of quartz and feldspar (albite) grains, subordinate biotites, muscovites, lithic fragments containing the aforementioned minerals, and accessory ilmenite, apatite and zircon, originating from the nearby metamorphic basement units. The greenschist metamorphic albites are characterized by intensive sericitization and minor growth of epidote. The main portion of the sediment can be characterized as poorly sorted coarse sand comprised of sub-angular to sub-rounded, sub-spherical grains (Fig. 4a). The sand contains 26–48% feldspar (plagioclase) and can be classified as an arkose. The porosity of the undeformed host sediment ranges between 39 and 45%, and can be attributed to lack of cementation and insignificant compaction due to shallow burial depth. The current overburden of the sampled sands is some 30 m, and most probably never exceeded roughly 150 m (corresponding to ca. 3–5 MPa overburden pressure), as these basin margin areas ceased to subside shortly after the deposition of this unit in the middle Miocene (Brix and Pascher, 1994; Strauss et al., 2006). Generally, the grains in the host sediment are intact and do not show signs of indentation or abundant grain breakage.

4.2. Microstructures in deformation bands

In the deformation bands with displacement between 0.5 and 8 cm, equivalent to a shear strain γ (=displacement/band width) between 0.5 and 4, we can observe an increase of fine grained minerals within the matrix. In BSE images (Fig. 4b), the matrix minerals can be identified as identical to the larger sized clasts, i.e. predominately quartz, feldspar and phyllosilicates. These 2–20 μm sized grains are dispersed in the pore space, without any cement or coating (Fig. 5e). Quartz clasts show evidence of grain flaking (Fig. 5a) and mechanical abrasion of material at acute and serrate edges. The porosity is reduced from 42% in the host sediment to 30–35% in the deformation band. Intragranular fracturing of any kind of minerals is rare, and affects preferably polymineralic aggregates (Fig. 5c) or strongly sericitized plagioclase grains (Fig. 5d and e).

For comparison Fig. 4c shows a deformation band with 60 cm offset at 2.5 cm width, corresponding to a γ of 24. In this zone, the porosity is reduced to 24%, i.e. a reduction of ca. 20% with respect to the undeformed host sediment (Fig. 4c). From BSE images, an increase of fine grained matrix material and a general reduction of grain size is evident. The matrix consists of fine grained mica (sericite), as well as quartz and feldspar flakes. Quartz shows flaking along conchoidal fractures (Fig. 5a) or intragranular fractures (Fig. 5b). Feldspar undergoes fracturing along crystallographic, orthogonal planes, and indicates strong mechanical abrasion, expelling sericite and epidote along the grain boundaries

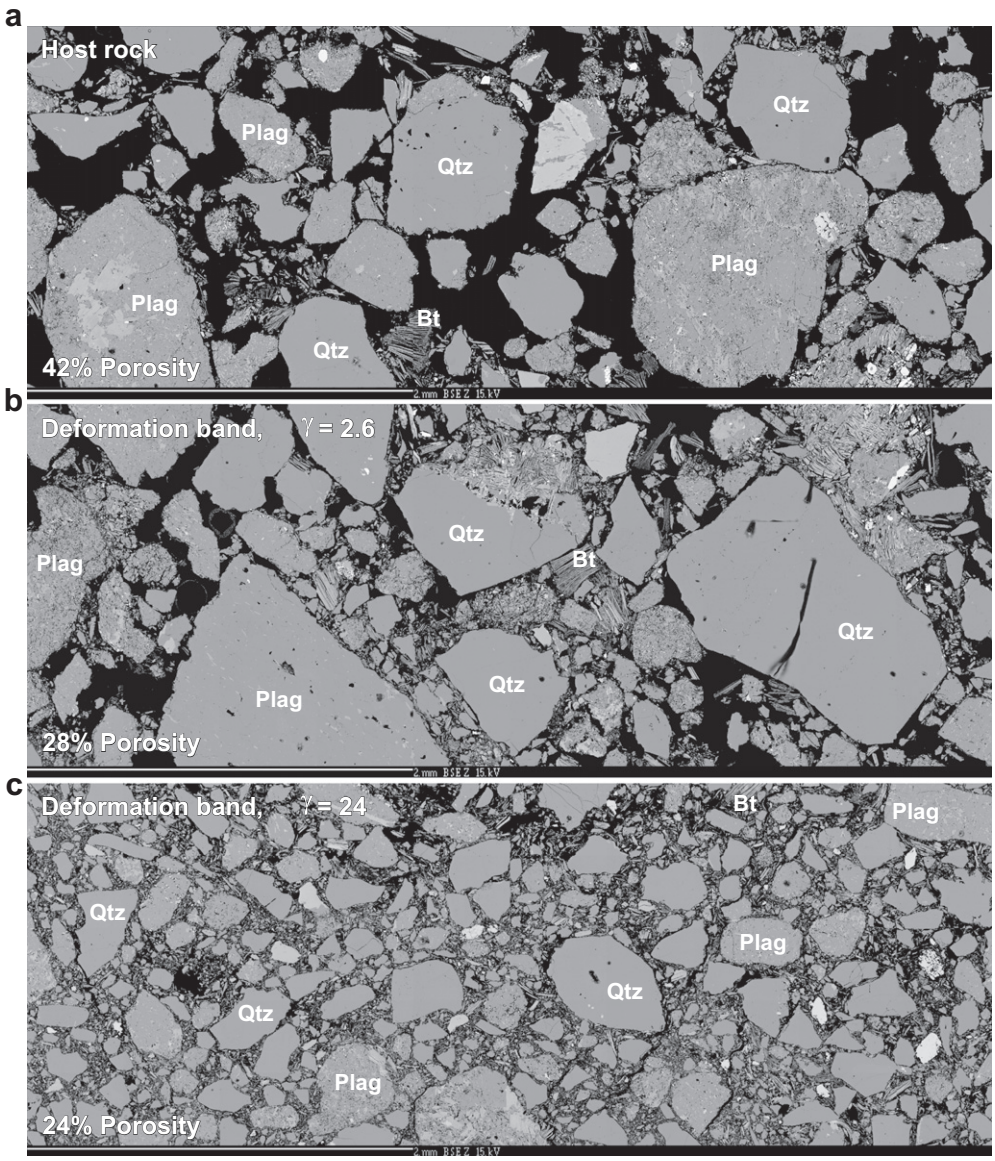

Fig. 4. EPMA BSE images of microstructures from (a) host sediment and deformation bands with (b) 4 cm displacement and (c) 60 cm displacement. Mineral abbreviations for quartz (Qtz), plagioclase (Plag), biotite (Bt), epidote (Ep) and sericite (Ser) are used also in Fig. 5.

(Fig. 5f). Lithic fragments composed of the primary metamorphic paragenesis (Fig. 5c), in this case quartz and mica aggregates, fracture along grain boundaries, thereby releasing quartz clasts of approx. 10–25 μm diameter. Within the width of a thin section, we observe strong variations in grain size and matrix content across this zone, which results in a banding perpendicular to the shear direction. In areas of smaller grain size also an increase in fine grained matrix material occurs; in these zones the larger clasts are predominately quartz grains (Fig. 4c).

4.3. Grain size analysis

Grain size distribution was measured from 5 × 2 mm sized BSE images of representative areas in the undisturbed host sediment, and two types of deformation bands with different shear strain (Fig. 4). An increase in silt sized grains from 5% in the host sediment to 7% in a deformation band with $\gamma = 2.6$, and finally to 18% in a deformation band with $\gamma = 24$ (i.e. 60 cm of displacement) can be observed (Fig. 6a). Cumulative distributions shown in log–log space (Fig. 6b) show a trend toward a linear distribution with a higher power law exponent (from $D = 0.68$ to $D = 0.79$) in the deformation bands with increasing strain. This corresponds to the comminution of larger grains (quartz, feldspar and lithic fragments) and the increase in medium to fine grains content (5–20 μm grain diameter).

In order to determine whether both quartz and feldspar contribute equally to the increase in fine grains content, we analyzed the grain size distribution of both minerals separately. Using binary images (examples are shown in Fig. 7) produced from phase cluster analysis of host sediment and deformation band (with $\gamma = 24$) we calculated exceedence frequency-grain area diagrams (Torabi and Fossen, 2009; Rawling and Goodwin, 2003) for each mineral (Fig. 8). The grain size distributions of quartz and feldspar are similar in the host sediment, although the curve for feldspar has a steeper slope indicating a larger amount of fine to medium grains than quartz. In contrast, the distributions are significantly different in the deformation band. The slope for quartz is only moderately steeper than in the host sediment, and shows the same characteristic kink around 0.1 mm^2 grain area (Fig. 8a). In the deformation band feldspar has a nearly linear distribution at a markedly higher slope ($D = 0.75$), with a larger increase from the

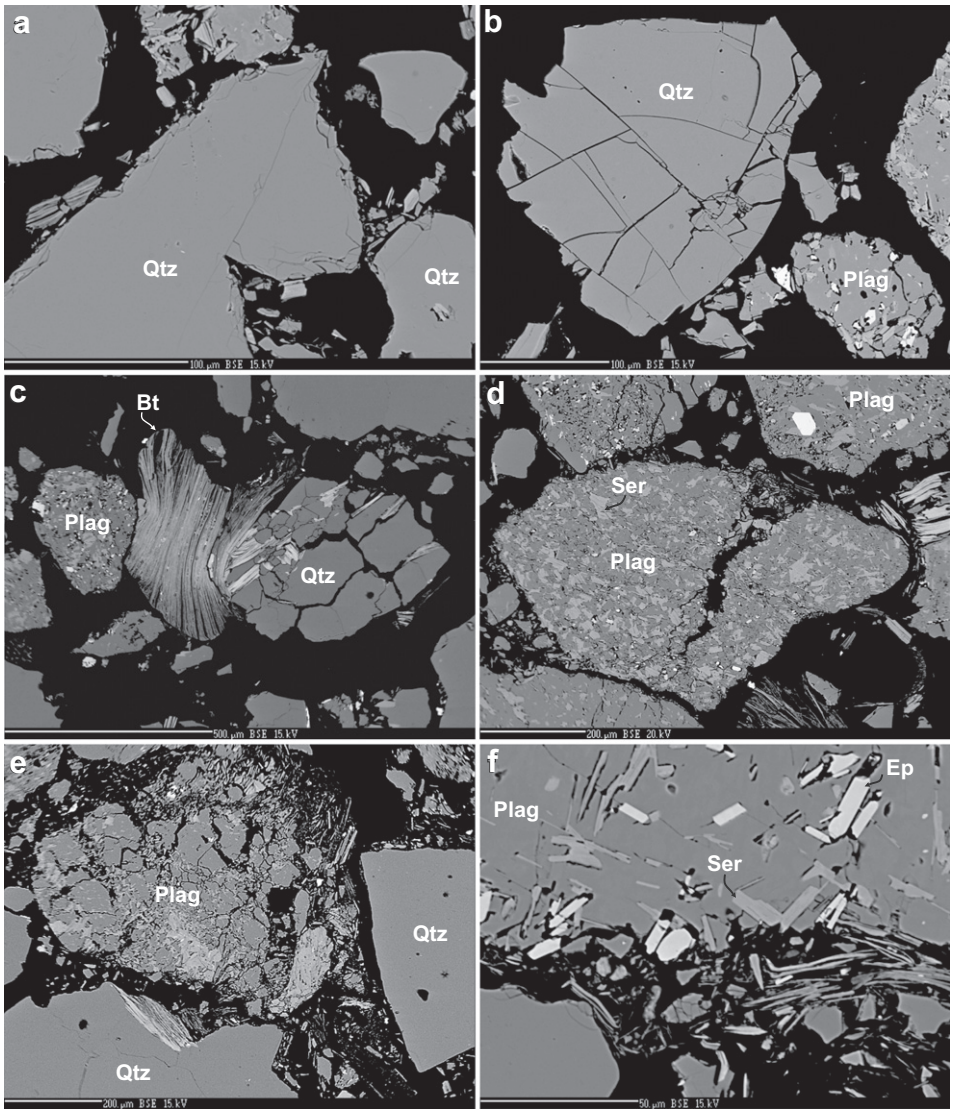

Fig. 5. EPMA BSE images of microstructural details observed in small strain ($\gamma = 2.6$) deformation bands (a, c, d, e) and large strain deformation bands (b, f, $\gamma = 24$). Quartz grains show flaking (a) and intragranular fracturing (b). Quartz aggregates break along grain boundaries, while biotite is sliced along cleavage planes (c). Strongly sericitized feldspar disintegrates by intragranular fractures in deformation bands (d), decomposing to fragments of feldspar and sericite (e). Mechanical abrasion of sericitized feldspar releases 5–20 μm sized needles of sericitic mica (f).

distribution in the host sediment in comparison to quartz, indicating a more efficient fracturing of the intermediate-sized grains.

4.4. Bulk and mineral chemistry of deformation bands and host sediment

The bulk major as well as trace element compositions of deformation bands were analyzed along with their corresponding host sediments (Table 1). The whole-rock composition (10 major and 21 trace elements) of a deformation band with 2 cm displacement ($\gamma = 2.6$) is plotted against the composition of the adjacent host material in Fig. 9a; likewise, element abundances of a deformation band having 60 cm of displacement ($\gamma = 24$) is compared to the neighboring sediment composition in Fig. 9b. The linear distribution of elements in the diagrams reflects a well-defined positive correlation between both samples of deformation bands and the respective host material.

In addition to the bulk geochemical analyses, compositions of mineral grains from the undisturbed sediment were compared to grains from the two types of deformation bands. Feldspar compositions ($Or_{0.5}Ab_{96.8}An_{2.7}$) of the larger grains in the host sediment are identical to compositions of the small feldspar-flakes and -grains that can be found in the matrix of the deformation bands (Table 2). Likewise, the sericite inclusions inside large feldspar clasts show identical chemical composition to the small loose sericite grains in the matrix of the deformation bands. The large detrital muscovite grains which are present in both deformation bands and host sediments are quite distinctively distinguishable from the small sericites, having higher amounts of FeO and TiO_2 and less SiO_2 (Table 2). The data confirm grain-disaggregation and cataclasis within the deformation bands, which are unaffected by chemical alterations or precipitation of clay minerals.

5. Discussion

5.1. Mechanical and chemical processes during deformation in arkosic sands

The presented microstructures from deformation bands in unconsolidated arkosic sands show no signs of cementation, or

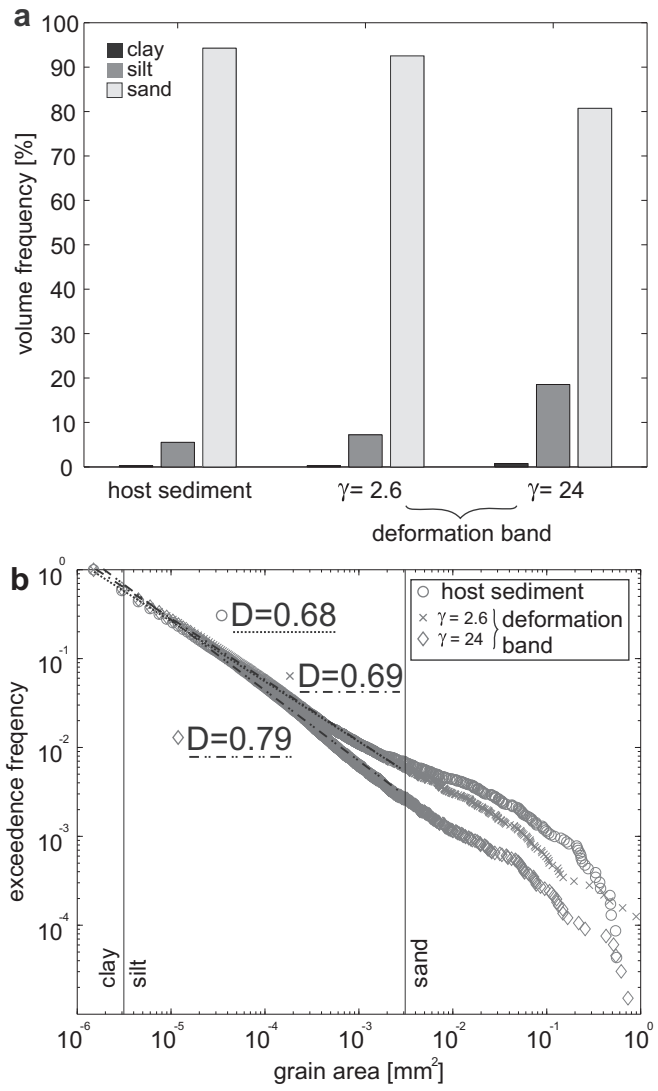

Fig. 6. Comparison of the grain size data of host sediment and deformation bands from EPMA BSE images (Fig. 2). (a) Increase in silt sized particles from 5% in the host sediment to 7% in the deformation band with low shear strain and 18% in the band with high shear strain. (b) Plot of exceedence frequency (normalized number of particles larger than the respective value) against grain area. Number of sand sized particles decreases from host sediment to deformation band with increasing strain. Power law exponents (D) are calculated by nonlinear least square fitting (dashed lines) of the logarithmically binned original data <0.002 mm^2.

pressure solution. In-situ mobilization of carbonate and precipitation in the pore space was impossible, due to the lack of carbonate particles or micritic carbonate matrix in the sediments. In the same way, no generation of quartz cements or solution seams have been found, neither in the deformation bands, nor in the undeformed host rock. Furthermore, fault sealing due to clay mineral accumulation can in this case be excluded by definition, as no clay minerals were detected in the studied BSE images. Since the bulk geochemical correlation of deformation bands and undisturbed host sediments clearly points to an isochemical deformation process, the enrichment of mineral phases which are not derived from the primary host sediments, as well as leaching, removal or infiltration of selective minerals (as described e.g. by Aydin et al., 2006) can be ruled out for our samples. Other authors assume that shear heating causes the growth of clay minerals in loose sands during coseismic rupturing (Balsamo and Storti, 2011) or observe entrainment of fine grained beds and mixing in the deformation band (e.g. Loveless et al., 2011). In contrast, the fine grained phyllosilicates in our samples are fine grained sericitic mica derived from inclusions in detrital feldspar grains altered under greenschist facies metamorphic conditions.

Based on the detailed microstructural and bulk-, as well as mineral geochemical considerations, it can be shown that grain size reduction in the investigated deformation bands and deformation bands is achieved by mainly grain flaking and intragranular fracturing. Furthermore, the mechanical breakdown of sericitized feldspar grains leads to fragmentation of these minerals and the release of single sericites that accumulate within the fine grained matrix (5–20 μm grain diameter) of the deformation bands. The chemical composition of these fine grained micas differs from the larger detrital muscovite and biotite grains (Table 2). This indicates the absence of significant compositional variance, loss or gain, or elemental fractionation between host sediments and deformation bands, and confirms the microstructural observations in favor of an isochemical deformation process without detectable precipitation or solution of material, independent on the finite shear strain accumulated along the structure.

The investigated outcrop comprises deformation bands with different amount of displacement and width. In addition to thin (1–2 cm thickness) bands with no or only some few cm offset, subparallel strands of deformation bands accumulated several dm to m of displacement by broadening of the bands and formation of new bands adjacent to the existing one (Fig. 2). Other deformation bands record more than 50 cm displacement along an only 2–5 cm thick zone. Even though the latter type of structures is not in full accordance with the original definition of deformation bands (Aydin, 1978), from our microstructural and chemical analysis, we cannot draw a clear distinction between bands of low and high shear strain. In both investigated types of deformation bands, conchoidal fractures producing small flakes expelled from the grain margins, as well as fractures transecting the entire grain are developed. However, with larger shear displacement, the abundance of flaking and fracturing of grains increases. Especially the occurrence of intragranular fractures of quartz single crystals is more frequent with larger shear strain. From separate grain size analysis of quartz and feldspar, we observe a more efficient fracturing of the weaker feldspar grains (Fig. 8) than that of quartz, and an associated release of sericite into the matrix (Fig. 5f). Notably, the calculated power law exponents for the grain size distributions in the deformation bands with $\gamma = 24$ are markedly lower than those reported from similar structures in uncemented feldspar-rich sands (i.e. $D = 1.6–2.0$) by Balsamo and Storti (2011). Instead, our values are more close to those measured in laboratory experiments (i.e. $D = 0.4–0.5$, Torabi et al., 2007) on quartz-rich sand, or in unconsolidated lithic arkose sands (i.e. $D = 0.6–1.1$, Rawling and Goodwin, 2003). All these datasets with similar D values show a consistent flattening of the particle size distributions within the analyzed shear bands in accordance to the data presented here. This flattening indicates a destruction of medium sized particles (Rawling and Goodwin, 2003), which are preferably affected by cataclasis between larger grains, while finer grained material is rather generated by spalling and flaking. Even though experimental studies indicate an increase in cataclastic grain fracturing with increasing normal stress (e.g. Marone and Scholz, 1989; Torabi et al., 2007), our data suggest that this process may also be triggered by higher shear strain, and is more pronounced in weaker materials (e.g. feldspar or lithic fragments).

According to the "Cam cap model" (Schultz and Siddharthan, 2005), yielding and the formation of deformation bands in porous rocks is strongly related to the physical properties of the host rock. In unconsolidated coarse sand, in which porosity and water content

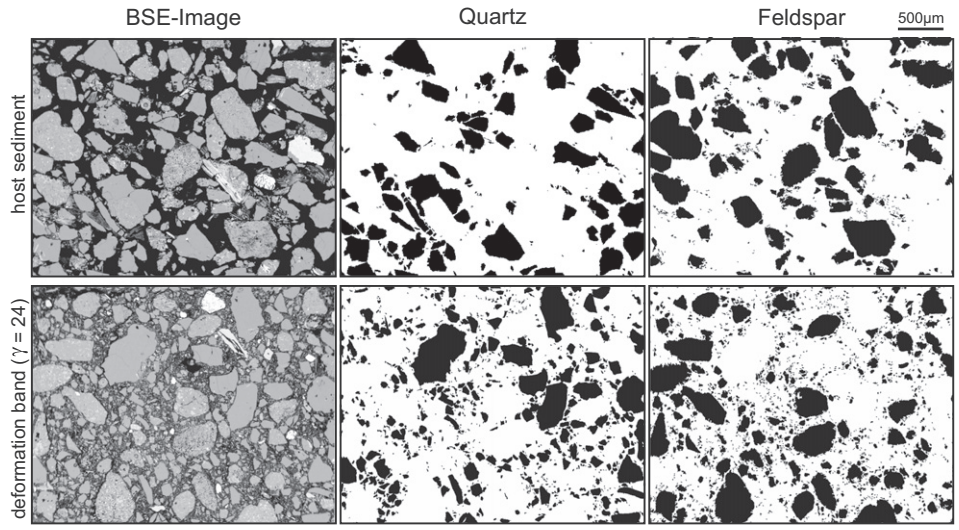

Fig. 7. BSE images and corresponding binary images of quartz and feldspar from host sediment and deformation band (sample STG07), used for separate grain size analyses (Fig. 8). Only particles >50 µm^2 are shown in binary images.

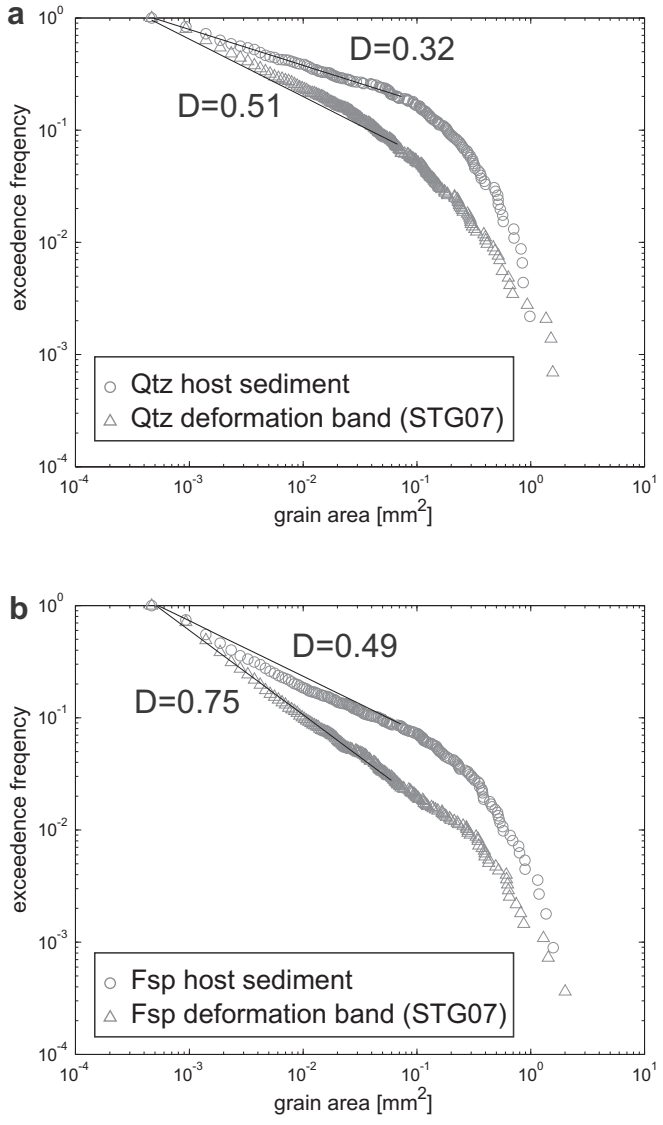

Fig. 8. Grain size distribution of a) quartz and b) feldspar in host sediment and deformation band. Power law exponents (D) are calculated by nonlinear least square fitting (solid lines) of the logarithmically binned original data <0.1 mm^2.

reduce the yield strength of the material, compaction and grain size reduction require less confining pressure (and thus overburden) than in consolidated, well cemented sandstones (Zhang et al., 1990). In detail, the porosity (~40%) and average grain size (1–1.5 cm) of our samples correspond to a critical pressure of only

Table 1
Representative XRF bulk major and trace element compositions of host sediments and deformation bands from St. Georgen.

	Host	DB STG06	Host	DB STG07
In wt.%				
SiO_2	73.7	73.8	75.8	74.5
TiO_2	0.48	0.49	0.27	0.35
Al_2O_3	13.3	13.2	12.9	13.5
Fe_2O_3[a]	2.31	2.30	1.65	1.89
MnO	0.04	0.04	0.02	0.03
MgO	0.86	0.84	0.64	0.71
CaO	1.20	1.14	0.94	1.03
Na_2O	3.87	3.74	4.01	4.08
K_2O	1.77	1.76	1.65	1.72
P_2O_5	0.20	0.19	0.10	0.13
LOI	1.54	1.63	1.30	1.44
Total	99.3	99.1	99.3	99.4
In ppm				
Sc	8.4	7.7	5.5	7.0
V	52.4	51.9	41.6	46.6
Cr	21.6	20.3	14.4	16.8
Ni	6.8	7.7	4.9	5.7
Cu	4.4	5.5	2.8	3.7
Zn	39.7	41.6	31.2	34.3
Ga	12.3	12.0	10.9	12.1
As	11.2	12.9	9.6	10.8
Rb	55.4	55.9	50.1	52.9
Sr	323	304	321	327
Y	17.3	16.7	9.3	13.2
Zr	190	178	97	122
Nb	6.9	7.3	3.7	5.0
Mo	0.4	0.4	0.5	0.4
Ba	703	674	699	699
La	65.0	71.7	37.8	46.8
Ce	117	121	62	79
Nd	54.9	50.8	30.8	37.8
Pb	11.3	12.1	11.0	11.6
Th	9.0	9.1	1.8	3.7
U	5.1	4.6	4.2	4.9

DB – deformation band; STG06: $\gamma = 2.6$; STG07: $\gamma = 24$; LOI – loss on ignition.
[a] Total iron.

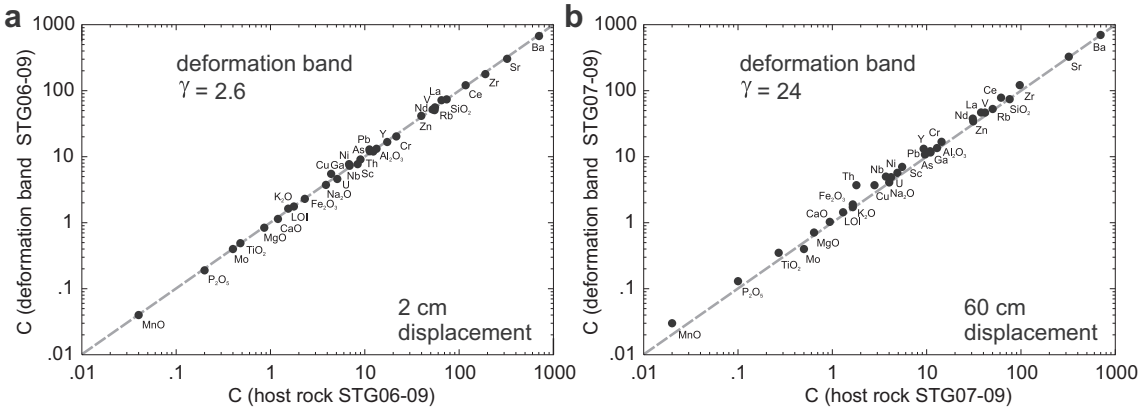

Fig. 9. Representative element concentrations (C) of a deformation band with (a) $\gamma = 2.6$ and (b) $\gamma = 24$ plotted against the composition of the respective adjacent host sediment.

ca. 2–4 MPa (using Equation (3) of Schultz et al., 2010), which is also in line with the data compiled by Zhang et al. (1990). Thus, in the presence of an equally low differential stress the observed shear deformation bands may have formed even below 2–4 MPa confining pressure corresponding to only some 100–150 m of burial depth.

5.2. Implications for reservoir properties

Sources of porosity and permeability reduction in deformation bands and faults in friable sediments may be, in addition to formation of clay minerals, the precipitation of carbonate, quartz or clay minerals from a fluid migrating preferentially through these deformation zones. In arid climates, deformation bands have been identified as conductors for fluid in the vadose zone (Wilson et al., 2003). In contrast, the distribution of iron-oxide staining along some of the deformation bands in the studied outcrop (Fig. 3b) indicates that the permeability is reduced within the bands. Nevertheless, at other locations within the same quarry (Figs. 2 and 3a), the staining does not show any retention by the deformation bands. These apparently contradicting observations might be due to differences in the orientation of the conjugate deformation bands relative to the direction of fluid flow, which probably was more vertical in the uppermost part of the succession (with conjugate deformation bands retaining Fe-hydroxide fluids, Fig. 3b), and more horizontal in the lower part (Fig. 3a), as proposed by Fossen and Bale (2007).

Table 2
Representative EPMA analyses of host sediment and deformation band minerals from St. Georgen (in wt.%).

	Host feldspars		DB feldspars	
	Mean	Std. dev.	Mean	Std. dev.
SiO_2	68.2	0.31	68.2	0.30
Al_2O_3	19.5	0.20	19.8	0.54
CaO	0.3	0.23	0.2	0.15
Na_2O	11.3	0.15	11.2	0.21
K_2O	0.1	0.03	0.1	0.02
Total	99.5	0.28	99.7	0.38

	Host-feldspar incorp. sericite		DB sericites		Detrital muscovites	
	Mean	Std. dev.	Mean	Std. dev.	Mean	Std. dev.
SiO_2	48.0	0.42	47.9	0.64	46.1	0.33
TiO_2	0.1	0.05	0.1	0.05	0.8	0.09
Al_2O_3	31.4	0.75	31.1	0.65	31.2	0.95
FeO[a]	2.4	0.15	2.5	0.44	4.3	0.13
MgO	1.1	0.25	1.1	0.29	1.4	0.64
Na_2O	0.5	0.09	0.4	0.21	0.2	0.02
K_2O	10.2	0.27	10.3	0.29	10.6	0.34
Total	93.7	0.53	93.5	0.59	94.6	0.28

[a] Total iron is shown as FeO, number of analyses $n > 15$.

Owing to the small displacement, deformation bands are not detectable in seismic data, but could have consequences for compartmentalization and sealing of a hydrocarbon reservoir or an aquifer. As a result of the incomplete reservoir connectivity caused by these structures, production of hydrocarbons or groundwater may be affected significantly. Previous studies on the microstructural processes which cause fault sealing in siliciclastic rocks (e.g. Fisher and Knipe, 1998) concluded that impure sandstones with 15–40% clay content may host "phyllosilicates framework" fault rocks. The deformation bands documented in the present study are different in that the content of phyllosilicates in the matrix is much lower in the host material, but is increased by the release of phyllosilicates from feldspar grains during cataclasis. The mechanical grain size reduction is, in our observations, not accompanied by a chemical alteration of the host sediment, e.g. of feldspar to clay minerals. In conventional borehole geophysical measurements (e.g. γ-log), and if cuttings are analyzed for their bulk composition, such zones of low porosity due to mechanical enrichment of phyllosilicates could be difficult to detect due to the lack of mineralogical variations relative to the host sediment. However, our observation that the distribution of iron-hydroxide staining can be controlled by the presence of these deformation bands indicates that they may significantly influence fluid migration.

In summary, our findings indicate that porosity reduction in deformation bands can be achieved by cataclasis, which causes grain fracturing and grain disaggregation. This results in grain size reduction of involved minerals and, depending on the host paragenesis, selective enrichment of phyllosilicates, already in deformation bands with very little displacement. Further research on the mineralogy of clay sized material in the deformation bands, and their contribution to permeability reduction and Fe-hydroxide staining is currently undertaken on a larger number of samples from this outcrop.

6. Conclusions

Deformation bands with variable degree of displacement and shear strain were studied in friable arkosic sands. Comparing the grain size distribution of quartz and feldspar in the undisturbed host sediment and the deformation bands, a preferred fracturing and thereby increase in finer grains of feldspar is observed. Microstructural analysis revealed that this process additionally increases the amount of phyllosilicates in the matrix, as sericite inclusions in the feldspars are released by fracturing of their host grains. Increasing shear strain leads to a transition form spalling

from larger grains toward intragranular fracturing of both feldspar and quartz grains. The retention of Fe-hydroxide rich fluids along the deformation bands indicates that this process reduces permeability enough to create baffles for fluid migration. This example demonstrates that cataclasis of weak components can lead to fault sealing and reservoir compartmentalization at low burial depth.

Acknowledgments

The study was supported by the Austrian Science Fund (Projects V151-N22 and I201). We thank G. Habler for support on the FEG-SEM and M. Ebner for providing helpful advice about image analysis. Thorough and constructive reviews by A. Torabi and G. Rawling, as well as by L. Goodwin, C. Childs and P. Eichhubl on an earlier version of the manuscript and careful editorial work by T. Blenkinsop are gratefully acknowledged.

References

Allen, P.A., Allen, J.R., 2005. Basin Analysis: Principles and Applications, second ed. Blackwell Publishing, Oxford.

Antonellini, M.A., Aydin, A., Pollard, D.D., 1994. Microstructures of deformation bands in porous sandstones at Arches National Park, Utah. Journal of Structural Geology 16, 941–959.

Aydin, A., 1978. Small faults formed as deformation bands in sandstone. Pure and Applied Geophysics 116, 913–930.

Aydin, A., Borja, R.I., Eichhubl, P., 2006. Geological and mathematical framework for failure modes in granular rock. Journal of Structural Geology 28, 83–98.

Balsamo, F., Storti, F., 2010. Grain size and permeability evolution of soft-sediment extensional sub-seismic and seismic fault zones in high-porosity sediments from the Crotone basin, southern Apennines, Italy. Marine and Petroleum Geology 27, 822–837.

Balsamo, F., Storti, F., 2011. Size-dependent comminution, tectonic mixing, and sealing behavior of a "structurally oversimplified" fault zone in poorly lithified sands: evidence for a coseismic rupture? Geological Society of America Bulletin 123, 601–619.

Baud, P., Zhu, W., Wong, T.-F., 2000. Failure mode and weakening effect of water on sandstone. Journal of Geophysical Research 105, 16371–16389.

Baud, P., Klein, E., Wong, T.-F., 2004. Compaction localization in porous sandstones: spatial evolution of damage and acoustic emission activity. Journal of Structural Geology 26, 603–624.

Blenkinsop, T.G., 1991. Cataclasis and processes of particle size reduction. Pure and Applied Geophysics 136, 59–86.

Brix, F., Pascher, G., 1994. Geologische Karte der Republik Österreich 1:50 000, Blatt 77 Eisenstadt. Geological Survey of Austria, Vienna.

Cashman, S., Cashman, K., 2000. Cataclasis and deformation-band formation in unconsolidated marine terrace sand, Humboldt County, California. Geology 28, 111–114.

Cashman, S.M., Baldwin, J.N., Cashman, K.V., Swanson, K., Crawford, R., 2007. Microstructures developed by coseismic and aseismic faulting in near-surface sediments, San Andreas fault, California. Geology 35, 611–614.

Eichhubl, P., Taylor, W.L., Pollard, D.D., Aydin, A., 2004. Paleo-fluid flow and deformation in the Aztec Sandstone at the Valley of Fire, Nevada—evidence for the coupling of hydrogeologic, diagenetic, and tectonic processes. Geological Society of America Bulletin 116, 1120–1136.

Eichhubl, P., D'Onfro, P.S., Aydin, A., Waters, J., McCarty, D.K., 2005. Structure, petrophysics, and diagenesis of shale entrained along a normal fault at Black Diamond Mines, California—implications for fault seal. American Association of Petroleum Geologists Bulletin 89, 1113–1137.

El Bied, A., Sulem, J., Martineau, F., 2002. Microstructure of shear zones in Fontainebleau sandstone. International Journal of Rock Mechanics & Mining Sciences 39, 917–932.

Exner, U., Grasemann, B., 2010. Deformation bands in gravels: displacement gradients and heterogeneous strain. Journal of the Geological Society London 167, 905–913.

Fisher, Q.J., Knipe, R.J., 1998. Fault sealing processes in siliciclastic sediments. In: Jones, G., Fisher, Q.J., Knipe, R.J. (Eds.), Faulting, Fault Sealing and Fluid Flow in Hydrocarbon Reservoirs, pp. 117–134.

Fodor, L., 1995. From transpression to transtension: Oligocene–Miocene structural evolution of the Vienna Basin and the East Alpine–Western Carpathian junction. Tectonophysics 242, 151–182.

Fossen, H., Bale, A., 2007. Deformation bands and their influence on fluid flow. American Association of Petroleum Geologists Bulletin 91, 1685–1700.

Fossen, H., Schultz, R.A., Shipton, Z.K., Mair, K., 2007. Deformation bands in sandstone: a review. Journal of the Geological Society 164, 755–769.

Haied, A., Kondo, D., 1997. Strain localization in Fontainbleau sandstone: macroscopic and microscopic investigations. International Journal of Rock Mechanics & Mining Sciences 34, 1–13.

Loveless, S., Bense, V., Turner, J., 2011. Fault architecture and deformation processes within poorly lithified rift sediments, Central Greece. Journal of Structural Geology 33, 1554–1568.

Marone, C., Scholz, C.H., 1989. Particle-size distribution and microstructures within simulated fault gouge. Journal of Structural Geology 11, 799–814.

Rath, A., Exner, U., Tschegg, C., Grasemann, B., Laner, R., Draganits, E., 2011. Diagenetic control of deformation mechanisms in deformation bands in a carbonate grainstone. American Association of Petroleum Geologists Bulletin 95, 1369–1381.

Rawling, G.C., Goodwin, L.B., 2003. Cataclasis and particulate flow in faulted, poorly lithified sediments. Journal of Structural Geology 25, 317–331.

Rawling, G.C., Goodwin, L.B., Wilson, J.L., 2001. Internal architecture, permeability structure, and hydrologic significance of contrasting fault-zone types. Geology 29, 43–46.

Royden, L.H., 1985. The Vienna Basin: a thin-skinned pull-apart basin. In: Biddle, K.T., Christie-Blick, N. (Eds.), Strike-Slip Deformation, Basin Formation, and Sedimentation. SEPM Special Publication, vol. 37, pp. 319–338.

Sauer, R., Seifert, P., Wessely, G., 1992. Guidebook to excursions in the Vienna Basin and the adjacent Alpine–Carpathian thrustbelt in Austria. Mitteilungen der Österreichischen Geologischen Gesellschaft 85, 1–264.

Schmid, P.H., Harzhauser, M., Kroh, A., 2001. Hypoxic events on a middle Miocene carbonate platform of the Central Paratethys (Austria, Badenian, 14 Ma). Annalen des Naturhistorischen Museums in Wien 102A, 1–50.

Schultz, R.A., Siddharthan, R., 2005. A general framework for the occurrence and faulting of deformation bands in porous granular rocks. Tectonophysics 411, 1–18.

Schultz, R.A., Okubo, C.H., Fossen, H., 2010. Porosity and grain size controls on compaction band formation in Jurassic Navajo Sandstone. Geophysical Research Letters 37, L22306. http://dx.doi.org/10.1029/2010GL044909.

Sigda, J.M., Goodwin, L.B., Mozley, P.S., Wilson, J.L., 1999. Permeability alteration in small-displacement faults in poorly lithified sediments: Rio Grande Rift, Central New Mexico. In: Haneberg, W.C., Mozley, P.S., Moore, J.C., Goodwin, L.B. (Eds.), Faults and Subsurface Fluid Flow in the Shallow Crust. AGU Monograph, vol. 113, pp. 51–68.

Sternlof, K.R., Rudnicki, J.W., Pollard, D.D., 2005. Anticrack inclusion model for compaction bands in sandstone. Journal of Geophysical Research 110. http://dx.doi.org/10.1029/2005JB003764.

Sternlof, K.R., Karimi-Fard, M., Pollard, D.D., Durlofsky, L.J., 2006. Flow and transport effects of compaction bands in sandstone at scales relevant to aquifer and reservoir management. Water Resources Research 42, W07425. http://dx.doi.org/10.1029/2005WR004664.

Strauss, P., Harzhauser, M., Hinsch, R., Wagreich, M., 2006. Sequence stratigraphy in a classic pull-apart basin (Neogene, Vienna Basin). A 3D seismic based integrated approach. Geologica Carpathica 57, 185–197.

Torabi, A., Braathen, A., Cuisiat, F., Fossen, H., 2007. Shear zones in porous sand: insights from ring-shear experiments and naturally deformed sandstones. Tectonophysics 437, 37–50.

Torabi, A., Fossen, H., 2009. Spatial variation of microstructure and petrophysical properties along deformation bands in reservoir sandstones. American Association of Petroleum Geologists Bulletin 93, 919–938.

Tueckmantel, C., Fisher, Q.J., Knipe, R.J., Lickorish, H., Khalil, S.M., 2010. Fault seal prediction of seismic-scale normal faults in porous sandstone: a case study from the eastern Gulf of Suez rift, Egypt. Marine and Petroleum Geology 27, 334–350.

Wilson, J.E., Goodwin, L.B., Lewis, C.J., 2003. Deformation bands in non-welded ignimbrites: petrophysical controls on fault-zone deformation and evidence of preferential fluid flow. Geology 31, 837–840.

Zhang, J., Wong, T.-F., Davis, D.M., 1990. Micromechanics of pressure-induced grain crushing in porous rocks. Journal of Geophysical Research 95, 341–352.